JACS ARTICLES

Published on Web 08/24/2009

Tuning the Sign of Photoinduced Changes in Magnetization: Spin Transitions in the Ternary Metal Prussian Blue Analogue $Na_\alpha Ni_{1-x}Co_x[Fe(CN)_6]_\beta \cdot nH_2O$

Daniel M. Pajerowski,[†] Justin E. Gardner,[‡] Daniel R. Talham,*[,‡] and Mark W. Meisel*[,†]

Department of Physics and NHMFL, University of Florida, Gainesville, Florida 32611-8440, and Department of Chemistry, University of Florida, Gainesville, Florida 32611-7200

Received February 18, 2009; E-mail: talham@chem.ufl.edu; meisel@phys.ufl.edu

Abstract: Tuning the composition of the ternary transition-metal Prussian blue analogue $Na_\alpha Ni_{1-x}Co_x[Fe(CN)_6]_\beta \cdot nH_2O$ allows the sign of the photoinduced change in magnetization to be controlled. The parent cobalt hexacyanoferrate material is well-known to display photoinduced and thermal charge-transfer-induced spin transitions (CTISTs). Upon partial replacement of Co ion sites with Ni^{II}, irradiation with halogen light can cause either an increase or a *decrease* in magnetization, depending upon the extent of Ni^{II} substitution, the applied field, and the temperature. For all compositions with $x > 0$, photoexcitation generates new moments according to the same mechanism observed for the parent $x = 1$ compound. However, the presence of Ni^{II} introduces a superexchange of opposite sign, providing a mechanism for controlling the sign of the change in magnetization with applied light. Additionally, dilution of the spin-crossover material reduces the magnitude and hysteresis of the thermal CTIST effect. These effects can be qualitatively explained by simple mean-field models.

I. Introduction

The ability to purposefully tune magnetic properties of synthetic materials has motivated progress in the area of molecule-based magnets. A new class of magnetic coordination compounds was established when long-range magnetic order was discovered in Prussian blue[1] and its atomic and magnetic structures were elucidated,[2] leading to the notion that properties could be controlled by changing transition-metal ions within the parent cubic framework. Binary-metal Prussian blue analogues (PBAs), $A_\alpha M'[M(CN)_6]_\beta \cdot nH_2O$ (where A is an alkali-metal ion, M′ and M are transition-metal ions, and the values of α, β, and n depend upon the stoichiometry), and similar materials have been the subject of extensive research because of their diverse and exciting range of magnetic properties.[3] Room-temperature magnetic order,[4] photoinduced magnetization,[5] thermal charge-transfer-induced spin transitions (CTISTs),[6] photoinduced tuning of magnetic coupling,[7] anisotropic photoinduced magnetism in thin films,[8] and linkage isomerism[9] are among the phenomena observed in this class of compounds.

Photoinduced magnetism, which was discovered by Hashimoto and co-workers in $K_{0.2}Co_{1.4}[Fe(CN)_6] \cdot 6.9H_2O$, has proven to be one of the more fascinating features of PBAs.[5a] Briefly, at low enough temperatures, incident light can cause an electron

[†] Department of Physics and NHMFL.
[‡] Department of Chemistry.

(1) (a) Davidson, D.; Welo, L. A. *J. Phys. Chem.* **1928**, *32*, 1191. (b) Holden, A. N.; Matthias, B. T.; Anderson, P. W.; Lewis, H. W. *Phys. Rev.* **1956**, *102*, 1463. (c) Bozorth, R. M.; Williams, H. J.; Walsh, D. E. *Phys. Rev.* **1956**, *103*, 572. (d) Ito, A.; Suenaga, M.; Ôno, K. *J. Chem. Phys.* **1968**, *48*, 3597.
(2) (a) Buser, H. J.; Schwarzenbach, D.; Petter, W.; Ludi, A. *Inorg. Chem.* **1977**, *16*, 2704. (b) Day, P.; Herren, F.; Ludi, A.; Güdel, H. U.; Hulliger, F.; Givord, D. *Helv. Chim. Acta* **1980**, *63*, 148.
(3) (a) Dunbar, K. R.; Heitz, R. A. *Prog. Inorg. Chem.* **1997**, *45*, 283. (b) Verdaguer, M.; Girolami, G. S. In *Magnetism: Molecules to Materials V*; Miller, J. S., Drillon, M., Eds.; Wiley-VCH: Weinheim, Germany, 2005; p 283. (c) Pokhodnya, K.; Bonner, M.; Her, J.-H.; Stephens, P.; Miller, J. *J. Am. Chem. Soc.* **2006**, *128*, 15592. (d) Miller, J. *Dalton Trans.* **2006**, 2742. (e) Verdaguer, M.; Gatteschi, D. C. R. *Chimie* **2008**, *11*, 1083. (f) Pokhodnya, K.; Dokukin, V.; Miller, J. *Inorg. Chem.* **2008**, *47*, 2249.
(4) (a) Ferlay, S.; Mallah, T.; Ouahès, R.; Veillet, P.; Verdaguer, M. *Nature* **1995**, *378*, 701. (b) Gadet, V.; Mallah, T.; Castro, I.; Verdaguer, M.; Veillet, P. *J. Am. Chem. Soc.* **1992**, *114*, 9213. (c) Mallah, T.; Thiébaut, S.; Verdaguer, M.; Veillet, P. *Science* **1993**, *262*, 1554. (d) Taliferro, M.; Thorum, M.; Miller, J. *Angew. Chem., Int. Ed.* **2006**, *45*, 5326.
(5) (a) Sato, O.; Iyoda, T.; Fujishima, A.; Hashimoto, K. *Science* **1996**, *272*, 704. (b) Bleuzen, A.; Lomenech, C.; Escax, V.; Villain, F.; Varret, F.; Cartier dit Moulin, C.; Verdaguer, M. *J. Am. Chem. Soc.* **2000**, *122*, 6648. (c) Cartier dit Moulin, C.; Villain, F.; Bleuzen, A.; Arrio, M.-A.; Sainctavit, P.; Lomenech, C.; Escax, V.; Baudelet, F.; Dartyge, E.; Gallet, J.-J.; Verdaguer, M. *J. Am. Chem. Soc.* **2000**, *122*, 6653. (d) Champion, G.; Escax, V.; Cartier dit Moulin, C.; Bluezen, A.; Villian, F.; Baudelet, F.; Dartyge, E.; Verdaguer, M. *J. Am. Chem. Soc.* **2001**, *123*, 12544. (e) Goujon, A.; Roubeau, O.; Varret, F.; Dolbecq, A.; Bleuzen, A.; Verdaguer, M. *Eur. Phys. J. B* **2000**, *14*, 115. (f) Goujon, A.; Varret, F.; Escax, V.; Bleuzen, A.; Verdaguer, M. *Polyhedron* **2001**, *20*, 1347. (g) Hanawa, M.; Moritomo, Y.; Kuriki, A.; Tateishi, J.; Kato, K.; Takata, M.; Sakata, M. *J. Phys. Soc. Jpn.* **2003**, *72*, 987. (h) Bleuzen, A.; Escax, V.; Itié, J.-P.; Münsch, P.; Verdaguer, M. C. R. *Chimie* **2003**, *6*, 343. (i) Yoo, J.-W.; Edelstein, R.; Lincoln, D.; Raju, N.; Xia, C.; Pokhodnya, K.; Miller, J.; Epstein, A. *Phys. Rev. Lett.* **2006**, *97*, 247205. (j) Brinzei, D.; Catala, L.; Mathoniere, C.; Wernsdorfer, W.; Gloter, A.; Stephan, O.; Mallah, T. *J. Am. Chem. Soc.* **2007**, *129*, 3778. (k) Yoo, J.-W.; Edelstein, R.; Lincoln, D.; Raju, N.; Epstein, A. *Phys. Rev. Lett.* **2007**, *99*, 157205. (l) Li, D.; Clérac, R.; Roubeau, O.; Harté, E.; Mathonière, C.; Le Bris, R.; Holmes, S. M. *J. Am. Chem. Soc.* **2008**, *130*, 252. (m) Bleuzen, A.; Marvaud, V.; Mathoniere, C.; Sieklucka, B.; Verdaguer, M. *Inorg. Chem.* **2009**, *48*, 3453.

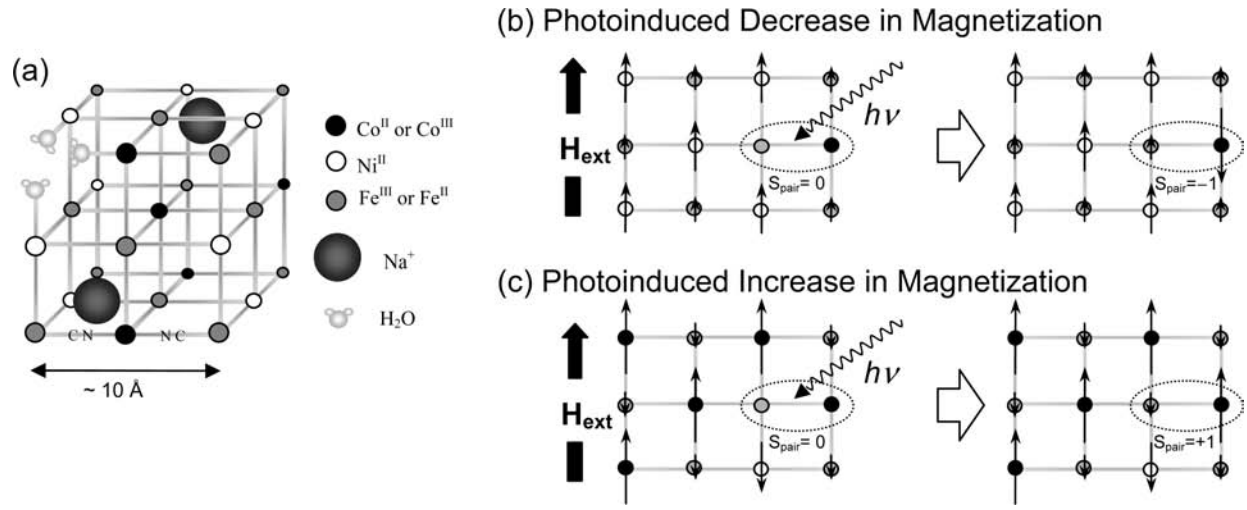

Figure 1. (a) Structural model for $Na_\alpha Ni_{1-x}Co_x[Fe(CN)_6]_\beta \cdot nH_2O$. (b) Decrease in the magnetization upon photoexcitation of a Ni-dominated material when there is atomic mixing and the spins are in an ordered state dictated by the exchange interactions $J_{NiFe} > 0$ and $J_{CoFe} < 0$. (c) The usual increase in the magnetization with photoexcitation of a sufficiently Co-dominated material.

to transfer from Fe^{II}(LS, $S = 0$) to Co^{III}(LS, $S = 0$), yielding long-lived metastable Fe^{III}(LS, $S = {}^1/_2$)−CN−Co^{II}(HS, $S = {}^3/_2$) pairs that couple antiferromagnetically and give rise to an observed increase in magnetization. An impressive body of work has elucidated the details of the thermal and optical CTIST effects in this series of compounds, $A_\alpha Co[Fe(CN)_6]_\beta \cdot nH_2O$ (A = Na, K, Rb, Cs).[5]

During an investigation of photoinduced magnetism in $A_\alpha Co[Fe(CN)_6]_\beta \cdot nH_2O$ thin films, workers in our laboratories discovered that nanometer-scale thin films undergo a photoinduced *decrease* in magnetization for a specific orientation of the film in the applied magnetic field.[8a] With the applied field parallel to the film, the commonly observed photoincrease is observed, but when the field is perpendicular to the film, the magnetization decreases with irradiation. A series of detailed studies indicated that the microscopic mechanism in the films is the same as for the bulk, that is, photoexcitation generates new moments.[8b−d] However, the film experiences a magnetic anisotropy not observable in the bulk solid state.

When our studies were extended to heterostructured thin films, new effects were observed.[10] When a layer of photoactive ferrimagnetic $Rb_\alpha Co[Fe(CN)_6]_\beta \cdot nH_2O$ is sandwiched between two layers of ferromagnetic $Rb_\alpha Ni[Cr(CN)_6]_\beta \cdot nH_2O$, photoexcitation can cause a *decrease* in magnetization for *all* film orientations. This observation is in contrast with the photodecrease observed in single-component films, for which the decrease is only observed in perpendicular orientations of the films with respect to the applied field. We conjectured that the photoeffect seen in the heterostructures may be due to heterogeneously distributed constituent ions at the interface between the two compounds, leading to competition between ferromagnetic and antiferromagnetic superexchange mechanisms.

In order to investigate this hypothesis, bulk materials in which Co or Fe ions present in the pure parent system can be exchanged for an ion that introduces a ferromagnetic component were considered. There has been previous interest in these so-called ternary metal PBAs, which are of the form $A_\alpha M''_{1-x}M'_x[M(CN)_6]_\beta \cdot nH_2O$ (where M″ and M′ occupy similar lattice sites, as determined by x), stemming from the additional effects that are sometimes observed, such as photoinduced magnetic-pole inversion,[11] dilution of spin crossover,[12] and magnets having different types of Neél order.[13] This ability to substitute different transition metals in the compound is due to the similar lattice parameters of the cubic binary PBAs. In addition to novel function, new insight into the underlying physical properties can be obtained through a study of these mixed PBAs.

In the present work, we report the synthesis of a ternary PBA of the form $Na_\alpha Ni_{1-x}Co_x[Fe(CN)_6]_\beta \cdot nH_2O$ in order to explore the origin of the photoinduced decrease in magnetization observed in the heterostructured thin films. The proposed structure is one in which a cubic iron sublattice interpenetrates a cubic sublattice containing a statistical mixture of cobalt and nickel ions (Figure 1a). The use of the sodium cation allows

(6) (a) Shimamoto, N.; Ohkoshi, S.-i.; Sato, O.; Hashimoto, K. *Inorg. Chem.* **2002**, *41*, 678. (b) Kosaka, W.; Nomura, K.; Hashimoto, K.; Ohkoshi, S.-i. *J. Am. Chem. Soc.* **2005**, *127*, 8590. (c) Escax, V.; Bleuzen, A.; Cartier dit Moulin, C.; Villain, F.; Goujon, A.; Varret, F.; Verdaguer, M. *J. Am. Chem. Soc.* **2001**, *123*, 12536.
(7) Ohkoshi, S.; Einaga, Y.; Fujishima, A.; Hashimoto, K. *J. Electroanal. Chem.* **1999**, *473*, 245.
(8) (a) Park, J.-H.; Čižmár, E.; Meisel, M. W.; Huh, Y. D.; Frye, F.; Lane, S.; Talham, D. R. *Appl. Phys. Lett.* **2004**, *85*, 3797. (b) Park, J.-H.; Frye, F.; Lane, S.; Čižmár, E.; Huh, Y. D.; Talham, D. R.; Meisel, M. W. *Polyhedron* **2005**, *24*, 2355. (c) Frye, F. A.; Pajerowski, D. M.; Lane, S. M.; Anderson, N. E.; Park, J.-H.; Meisel, M. W.; Talham, D. R. *Polyhedron* **2007**, *26*, 2281. (d) Frye, F. A.; Pajerowski, D. M.; Park, J.-H.; Meisel, M. W.; Talham, D. R. *Chem. Mater.* **2008**, *20*, 5706. (e) Yamamoto, T.; Umemura, Y.; Sato, O.; Einaga, Y. *J. Am. Chem. Soc.* **2005**, *127*, 16065.
(9) (a) Shriver, D. F.; Shriver, S. A.; Anderson, S. E. *Inorg. Chem.* **1965**, *4*, 725. (b) Brown, D. B.; Shriver, D. F.; Schwartz, L. H. *Inorg. Chem.* **1968**, *7*, 77. (c) Brown, D. B.; Shriver, D. F. *Inorg. Chem.* **1969**, *8*, 37. (d) House, J. E., Jr.; Bailar, J. C., Jr. *Inorg. Chem.* **1969**, *8*, 672. (e) Reguera, E.; Bertrán, J. A.; Nuñez, L. *Polyhedron* **1994**, *13*, 1619. (f) Martínez-Garcia, R.; Knobel, M.; Reguera, E. *J. Phys. Chem. B* **2006**, *110*, 7296.
(10) (a) Park, J.-H. Ph.D. Dissertation, University of Florida, Gainesville, FL, 2006. (b) Frye, F. A. Ph.D. Dissertation, University of Florida, Gainesville, FL, 2007.
(11) (a) Ohkoshi, S.-i.; Hashimoto, K. *J. Am. Chem. Soc.* **1999**, *121*, 10591. (b) Ohkoshi, S.-i.; Yorozu, S.; Sato, O.; Iyoda, T.; Fujishima, A.; Hashimoto, K. *Appl. Phys. Lett.* **1997**, *70*, 1040.
(12) Cafun, J.-D.; Londinière, L.; Rivière, E.; Bleuzen, A. *Inorg. Chim. Acta* **2008**, *361*, 3555.
(13) (a) Ohkoshi, S.; Iyoda, T.; Fujishima, A.; Hashimoto, K. *Phys. Rev. B* **1997**, *56*, 11642. (b) Ohkoshi, S.-i.; Sato, O.; Iyoda, T.; Fujishima, A.; Hashimoto, K. *Inorg. Chem.* **1997**, *36*, 268. (c) Ohkoshi, S.-i.; Hashimoto, K. *Phys. Rev. B* **1999**, *60*, 12820.

for clear thermal hysteresis,[6a] and the presence of Ni^{II} gives rise to ferromagnetic superexchange pathways between Ni^{II} and Fe^{III} characterized by an exchange constant similar in magnitude to that for Co^{II}−NC-Fe^{III} exchange.[14] The role of the ferromagnetic species in the photodecrease can be illustrated by considering the Ni-rich ($x \gtrsim 0$) and Ni-poor ($x \lesssim 1$) substitution regimes (Figure 1b,c). Although a similar mix of materials yielding $Co_{0.75}Ni_{0.75}[Fe(CN)_6]\cdot 6.8H_2O$ has already been reported elsewere,[15] the thermally and optically induced bistabilities of the spin states are not present because of the stoichiometry.

Our studies show that $Na_\alpha Ni_{1-x}Co_x[Fe(CN)_6]_\beta \cdot nH_2O$ bulk powder displays photoinduced magnetism that can be either *positive* or *negative*, depending upon the cobalt fraction $x = [Co]/([Co] + [Ni])$, the applied magnetic field, and the temperature. These observations are only the second report of a photoinduced *decrease* in magnetization for this class of photoswitchable coordination compounds. For the first time, the sign of the photoinduced change in magnetization can be controlled by tuning the chemical composition. Additionally, an x dependence is found for the ordering temperature, the coercive field, the amount of photoactive material, the magnitude of the thermal CTIST, and the width of the thermal CTIST hysteresis loop. We can qualitatively understand these results in the context of simple molecular field theories.

II. Experimental Details

A. Synthesis. Prussian blue analogues $Na_\alpha Ni_{1-x}Co_x[Fe(CN)_6]_\beta \cdot nH_2O$ were precipitated by treating 20 mL of 20 mM $Na_3Fe(CN)_6$ aqueous solutions with an equal volume of an aqueous solution containing a mixture of $NiCl_2$ and $CoCl_2$ (20 mM total transition metal) and NaCl (2 M). $Na_3Fe(CN)_6$(aq) was synthesized by oxidizing $Na_4Fe(CN)_6$(aq) with Cl_2(g) and used in situ.[6b] The concentration of Co^{II} in the precipitated solids, given by x, was controlled by varying the volume ratio of Co^{II}(aq) used during synthesis, defined as $x_{synthesis} = [Co^{II}]/([Co^{II}] + [Ni^{II}])$, while keeping the total transition-metal ion concentration at 20 mM. The reaction mixtures were stirred for 3 h in open atmosphere, and the microcrystalline powders were then isolated by centrifugation. The precipitates were rinsed three times with water and dried under a stream of nitrogen gas. Values of $x_{synthesis} = 0.00$ (**1**), 0.20 (**2**), 0.40 (**3**), 0.60 (**4**), 0.80 (**5**), and 1.00 (**6**) yielded compounds with $x =$ 0.00, 0.22, 0.45, 0.66, 0.87, and 1.00, respectively. Deionized water used in synthetic procedures was obtained from a Barnstead NANOpure system with a resistivity of at least 17.8 MΩ. All of the other reagents were purchased from Sigma-Aldrich or Fisher-Acros and used without further purification.

$Na_{0.27}Ni^{II}_{1.0}[Fe^{III}(CN)_6]_{0.73}[Fe^{II}(CN)_6]_{0.02}\cdot 5.0H_2O$ (1). IR (KBr): 2163 (vs, ν_{CN}), 2123 (m, ν_{CN}), 2079 (vw, ν_{CN}), 2043 (vw, ν_{CN}) cm^{-1}. EDS (Ni/Fe) 58.3:41.7. Anal. Calcd for $C_{4.5}H_{10.0}N_{4.5}O_{5.0}Na_{0.27}Ni_{1.0}Fe_{0.75}$: C, 17.21; H, 3.21; N, 20.08. Found: C, 17.16; H, 2.87; N, 19.33.

$Na_{0.31}Co^{II}_{0.22}Ni^{II}_{0.78}[Fe^{III}(CN)_6]_{0.74}[Fe^{II}(CN)_6]_{0.03}\cdot 4.4H_2O$ (2). IR (KBr): 2163 (vs, ν_{CN}), 2120 (m, ν_{CN}), 2095 (vw, ν_{CN}), 2045 (vw, ν_{CN}) cm^{-1}. EDS (Co/Ni/Fe) 12.4:45.6:42.0. Anal. Calcd for $C_{4.6}H_{8.8}N_{4.6}O_{4.4}Na_{0.31}Co_{0.22}Ni_{0.78}Fe_{0.77}$: C, 17.99; H, 2.88; N, 20.99. Found: C, 17.75; H, 2.84; N, 19.91.

$Na_{0.34}Co^{II}_{0.45}Ni^{II}_{0.55}[Fe^{III}(CN)_6]_{0.71}[Fe^{II}(CN)_6]_{0.05}\cdot 4.9H_2O$ (3). IR (KBr): 2162 (vs, ν_{CN}), 2120 (m, ν_{CN}), 2070 (w, ν_{CN}), 2041 (vw, ν_{CN}) cm^{-1}. EDS (Co/Ni/Fe) 26.1:31.9:42.0. Anal. Calcd for $C_{4.6}H_{9.8}N_{4.6}O_{4.9}Na_{0.34}Co_{0.45}Ni_{0.55}Fe_{0.76}$: C, 17.33; H, 3.13; N, 20.22. Found: C, 17.23; H, 2.95; N, 19.55.

$Na_{0.33}Co^{II}_{0.66}Ni^{II}_{0.34}[Fe^{III}(CN)_6]_{0.67}[Fe^{II}(CN)_6]_{0.08}\cdot 4.6H_2O$ (4). IR (KBr): 2161 (vs, ν_{CN}), 2119 (m, ν_{CN}), 2070 (w, ν_{CN}), 2038 (vw, ν_{CN}) cm^{-1}. EDS (Co/Ni/Fe) 38.3:20.1:41.6. Anal. Calcd for $C_{4.5}H_{9.2}N_{4.5}O_{4.6}Na_{0.33}Co_{0.66}Ni_{0.34}Fe_{0.75}$: C, 17.53; H, 3.012; N, 20.45. Found: C, 17.37; H, 2.88; N, 19.62.

$Na_{0.27}Co^{II}_{0.87}Ni^{II}_{0.13}[Fe^{III}(CN)_6]_{0.63}[Fe^{II}(CN)_6]_{0.10}\cdot 3.8H_2O$ (5). IR (KBr): 2161 (vs, ν_{CN}), 2117 (m, ν_{CN}), 2094 (m, ν_{CN}), 2041 (w, ν_{CN}) cm^{-1}. EDS (Co/Ni/Fe) 51.7:7.7:40.6. Anal. Calcd for $C_{4.4}H_{7.6}N_{4.4}O_{3.8}Na_{0.27}Co_{0.87}Ni_{0.13}Fe_{0.73}$: C, 18.25; H, 2.66; N, 21.28. Found: C, 17.90; H, 2.69; N, 20.25.

$Na_{0.31}Co^{II}_{1.0}[Fe^{III}(CN)_6]_{0.72}[Fe^{II}(CN)_6]_{0.04}\cdot 4.4H_2O$ (6). IR (KBr): 2160 (vs, ν_{CN}), 2115 (vw, ν_{CN}), 2094 (w, ν_{CN}), 2057 (vw, ν_{CN}) cm^{-1}. EDS (Co/Fe) 58.2:41.6. Anal. Calcd for $C_{4.6}H_{8.8}N_{4.6}O_{4.4}Na_{0.31}Co_{1.0}Fe_{0.76}$: C, 17.87; H, 2.89; N, 20.85. Found: C, 17.67; H, 2.54; N, 20.07.

B. Chemical and Structural Characterization. Energy-dispersive X-ray spectroscopy (EDS) and transmission electron microscopy (TEM) were performed on a JEOL 2010F instrument to establish transition-metal composition and particle size. Samples were deposited as methanol suspensions onto 400 mesh copper grids with holey carbon support films purchased from Ted Pella, Inc. Particle sizes were determined from the TEM images by measuring the edge length of more than 50 particles for each composition through the use of ImageJ imaging software.[16] A Thermo Scientific Nicolet 6700 spectrometer was used to record Fourier transform IR (FT-IR) spectra using KBr pellets or powder samples spread between NaCl plates. Combustion analysis to determine carbon, hydrogen, and nitrogen (CHN) percentages was performed by the University of Florida Spectroscopic Services laboratory.

To investigate the lattice constants and crystal structure, a Philips APD 3720 powder diffractometer, housed in the Major Analytical Instrument Center at the Univesity of Florida, was used to perform room-temperature X-ray diffraction (XRD) using a Cu Kα source. From the same samples used for all the other characterizations (including magnetometry), except for the $x = 1.00$ sample, of which only 0.6 mg was left by the time XRD was performed, 10−20 mg masses were mounted on glass slides and pressed onto squares of double-sided cellophane tape with areas of ~ 2.3 cm^2. The resulting diffractograms (Figures S1 and S2 in the Supporting Information) were used to model the structures by Rietveld refinement using the EXPGUI[17] interface for GSAS.[18] In order to approximate the complicated PBA structure, a single-phase model with $Fm\bar{3}m$ (No. 225) space-group symmetry was used. Specifically, the cobalt and nickel atoms were forced to occupy the same site. Atomic occupancies were set by the experimentally determined chemical formulas, except for the oxygen atoms of the interstitial waters, which were allowed to vary because the samples may have dehydrated or hydrated between synthesis and diffraction. The same site symmetries as in Prussian blue were used, with the iron vacancies replaced by the six coordinated oxygen atoms of the ligand water molecules.[2a] Placement of the oxygen atoms of the interstitial water molecules at the 32*f* Wyckoff position[5g] and a relatively small percentage at the 192*l* position was found to yield robust local minima during the refinement procedure.

C. Magnetic Measurements. Magnetic measurements were performed using a Quantum Design MPMS XL superconducting quantum interference device (SQUID) magnetometer. For photomagnetic measurements, a room-temperature halogen light source (∼1−2 mW) was used to introduce light into the sample chamber of the SQUID through a bundle of 10 optical fibers with ∼270 μm o.d. (Ocean Optics model 200). Powders were mounted on pieces of cellophane tape around plastic drinking straws to increase the optical cross-section for the photomagnetic studies. High-temperature data ($T > 100$ K) were taken using gelcaps as

(14) Juszczyk, S.; Johansson, C.; Hanson, M.; Ratuszna, A.; Małecki, G. *J. Phys.: Condens. Matter* **1994**, *6*, 5697.
(15) Kumar, A.; Yusuf, S. M. *Physica B* **2005**, *362*, 278.
(16) Rasband, W. S. *ImageJ*; U. S. National Institutes of Health: Bethesda, MD, 1997−2008; http://rsb.info.nih.gov/ij/.
(17) Toby, B. H. *J. Appl. Crystallogr.* **2001**, *34*, 210.
(18) Larson, A. C.; Von Dreele, R. B. *Los Alamos Natl. Lab., Rep. LAUR* **2000**, 86–748.

Table 1. Molecular Formulas and Unit Cell Parameters for Compounds **1**−**6**[23]

compound	x	proposed molecular formula	unit cell length (Å)
1	0.0	$Na_{0.27}Ni^{II}_{1.0}[Fe^{III}(CN)_6]_{0.73}[Fe^{II}(CN)_6]_{0.02}\cdot 5.0H_2O$	10.23(9)
2	0.22	$Na_{0.31}Co^{II}_{0.22}Ni^{II}_{0.78}[Fe^{III}(CN)_6]_{0.74}[Fe^{II}(CN)_6]_{0.03}\cdot 4.4H_2O$	10.24(9)
3	0.45	$Na_{0.34}Co^{II}_{0.45}Ni^{II}_{0.55}[Fe^{III}(CN)_6]_{0.71}[Fe^{II}(CN)_6]_{0.05}\cdot 4.9H_2O$	10.25(6)
4	0.66	$Na_{0.33}Co^{II}_{0.66}Ni^{II}_{0.34}[Fe^{III}(CN)_6]_{0.67}[Fe^{II}(CN)_6]_{0.08}\cdot 4.6H_2O$	10.26(8)
5	0.87	$Na_{0.27}Co^{II}_{0.87}Ni^{II}_{0.13}[Fe^{III}(CN)_6]_{0.63}[Fe^{II}(CN)_6]_{0.10}\cdot 3.8H_2O$	10.28(9)
6	1.0	$Na_{0.31}Co^{II}_{1.0}[Fe^{III}(CN)_6]_{0.72}[Fe^{II}(CN)_6]_{0.04}\cdot 4.4H_2O$	10.30(7)

the sample holders to accommodate additional sample mass. Backgrounds were subtracted from the data by using the measured mass susceptibility of similar sample holders. The same demagnetizing protocol, during which the magnetic field was oscillated to zero by successive ramps starting at 20 kG, was used for all of the low-field measurements at ∼10 G. Additionally, the magnet was allowed to relax for more than 2 h subsequent to demagnetization and prior to data taking. By using a commercial Toshiba THS118E Hall sensor calibrated in-house, we estimated differences of up to ∼1 G in the external fields applied to different samples, but for each specimen, the field was not changed between the light and dark states for the temperature sweeps, ensuring that any resulting effects were not a result of slight perturbations of the external field.

D. Mean-Field Calculations. Using simple mean-field approximations, we originally investigated the possible effects to be observed in the magnetization and subsequently refined the model after completing a series of experiments. In order to model the magnetic interactions, an approximation in which superexchange energies act as effective magnetic fields (so-called Weiss fields) was employed in a manner akin to that in previous work on similar materials.[11,13] In order to model the cooperative, thermally active CTIST event, a Bethe−Peierls−Weiss approximation to a phenomenological spin-crossover Hamiltonian was implemented.[19] Our numerical studies extend the previous work of others by allowing the high-spin fraction, n_{HS}, which is experimentally controlled by irradiation and temperature, to vary along with the relative metal concentration, x, which is dictated by the synthesis. Details of the calculations, including how x and n_{HS} were utilized to provide numerical results that are directly comparable to the experimental data, are described in the Supporting Information, including Figures S3 and S4.

III. Results

A. Synthesis. Compounds **1**−**6** having the general formula $Na_\alpha Co_x Ni_{1-x}[Fe(CN)_6]_\beta \cdot nH_2O$ were synthesized by varying the relative cobalt fraction $x_{synthesis}$ from 0.0 to 1.0 in steps of 0.2. The resultant chemical formulas given in Table 1 were determined from EDS, FT-IR, and CHN analyses. The Co, Ni, and Fe ratios were explicitly taken from the EDS results, because the signals for these ions were clean and reproducible. The percentages of C, H, and N were taken directly from combustion analyses. From the combustion results for the hydrogen content, the amount of oxygen was calculated by assuming that all of the hydrogen and oxygen were in H_2O molecules. The amount of Ni^{II} and Co^{II} present in the isolated compounds, x, closely tracked the fraction used in synthesis, $x_{synthesis}$, with a slight tendency for the materials to incorporate more Co^{II} (Table 1 and Figure 2). The color of the compounds also changed gradually from yellow to purple as the Co^{II} content increased (Figure S5 in the Supporting Information).

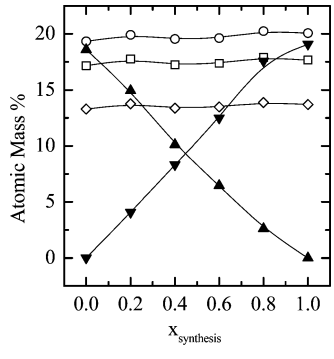

Figure 2. Measured atomic composition of carbon (□), nitrogen (○), iron (◇), nickel (▲), and cobalt (▼) for the compounds in Table 1 as a function of $x_{synthesis}$. Solid lines are guides for the eyes.

The relative ratios of Fe^{II} and Fe^{III} were estimated by fitting and subsequently integrating the cyanide stretching peaks in the FT-IR spectra associated with each species. Extinction coefficients of the cyanide stretching bands of the ternary PBA compounds were estimated from those measured for $Ni^{II}Fe^{III}$ and $Ni^{II}Fe^{II}$ PBA species (Figures S6 and S7 in the Supporting Information). The FT-IR spectrum of pure cobalt hexacyanoferrate displays peaks at 2163, 2120, 2090, and 2040 cm^{-1} corresponding to the cyanide stretches of the $Co^{II}Fe^{III}$(HS), $Co^{III}Fe^{II}$(LS), $Co^{II}Fe^{II}$, and linkage-isomerized $Co^{II}Fe^{II}$ phases, respectively.[20] The FT-IR spectrum of pure nickel hexacyanoferrate displays peaks at 2160 and 2125 cm^{-1} corresponding to the bridged and terminal cyanide of $Ni^{II}Fe^{III}$ PBA as well as peaks at 2079 and 2043 cm^{-1} corresponding to the same assignments for the reduced $Ni^{II}Fe^{II}$ sites.[21] As the concentration of Ni^{II} in the lattice was increased at the expense of Co^{II} ions, the intensities of the three peaks at 2120, 2090, and 2040 cm^{-1} decreased, while that of the peak at 2163 cm^{-1} remained relatively unchanged and a peak at 2125 cm^{-1} emerged. These intensity changes indicate both the reduction in the number of cobalt−iron pairs and the subsequent formation of nickel−iron pairs. The FT-IR spectra and the peak-fitting results can be found in Figure S8 in the Supporting Information. Finally, the amount of Na in the formulas was assigned by charge balance in conjunction with the previously discussed constraints, and, in each case, the assignment was consistent with the EDS and combustion analyses.[22]

The structure of the compounds as a function of x was investigated with TEM and powder XRD. For identical synthesis protocols except for the ratio of Co^{II}(aq) to Ni^{II}(aq), the equilibrium size of the particles evolved continuously, with the particles becoming larger as more Co^{II} ions are introduced into the lattice (Figure 3). Similarly, the unit cell constants changed continuously as x was varied from 0 to 1 (Figure 4). The continuous evolution of particle size, the absence of separate

(19) Hôo, B.; Boukheddaden, K.; Varret, F. *Eur. Phys. J. B* **2000**, *17*, 449.
(20) Ng, C. W.; Ding, J.; Gan, L. M. *J. Solid State Chem.* **2001**, *156*, 400.
(21) Sato, O. *J. Solid State Electrochem.* **2007**, *11*, 773.
(22) Because of the known problems of detecting light atoms, the EDS data were not exclusively used to determine the sodium content.
(23) Mass percentages of C, H, and N were taken explicitly from combustion analysis, and mass percentages of Co, Ni, and Fe were taken explicitly from EDS results.

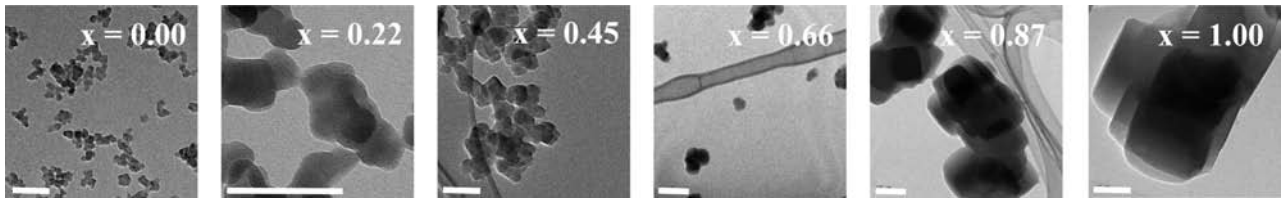

Figure 3. Typical TEM micrographs of the samples reported in Table 1 for different values of x. All scale bars shown are 100 nm. A continuous increase in equilibrium particle edge length is observed when cobalt ions are added to the extended networks. The average particle sizes from left to right are 15.6 ± 3.4, 26.5 ± 5.3, 28.7 ± 6.9, 38.7 ± 7.7, 117.2 ± 22.7, and 237.8 ± 40.1 nm.

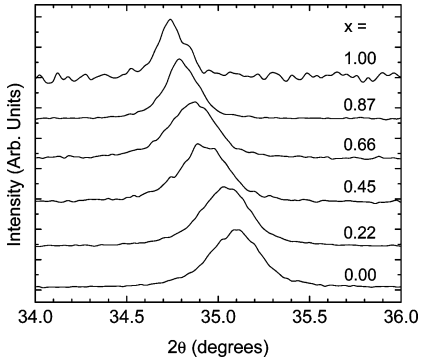

Figure 4. Room-temperature XRD patterns with background subtracted and intensity normalized to show the continuous evolution with x. The peak position shifts and the line width broadens as x decreases, reflecting the smaller particle size of the pure Ni−Fe analogue.

precipitates of the parent compounds, and the continuous evolution of the lattice constant without a change in the single-phase space group support the homogeneous mixing of the two ions within the lattice (Table 1 and Figures 3 and 4). Finally, some control over particle size for a given x value was possible by varying the concentration and the amount of time that the particles were in solution before isolation. However, we did not find observable changes in the magnetization, for given values of x, as a function of size within the regime studied.[24,25]

B. Low-Temperature Magnetization. The time dependences of the dc magnetic susceptibilities, $\chi = M/H$, during photoirradiation of the samples is shown in Figure 5a. The temperature dependence of the dc magnetic susceptibilities, $\chi(T)$, for $T =$ 2−30 K at ∼10 G for various x values, both before and after photoirradiation, are shown in Figure 5b. A clear bifurcation of the field-cooled (FC) and zero-field-cooled (ZFC) curves, with a peak in χ_{ZFC}-versus-T plots, was observed for all of the samples. The results of the Weiss mean-field calculations (described in the Supporting Information) are shown in Figure 5c. For the mean-field-calculated susceptibilities of the dark states, the value of the high-spin fraction, n_{HS}, is dictated by the amount of material measured to undergo spin crossover, whereas the calculated susceptibilities of the photoirradiated states use $n_{HS} = 1$, where all available material is in the high-spin state by definition.

All of the samples with $x > 0$ showed a change in magnetization due to applied light. Strikingly, at 5 K in a field of 10 G, the $x = 0.66$ sample showed a clear decrease in magnetization with photoirradiation in both the calculations and the experimental results. A photoinduced decrease in magnetization to a weaker extent was also observed in the $x = 0.45$ sample. The magnetization as a function of the applied magnetic field was measured for all of the compounds at $T = 2$ K for fields up to 70 kG, and these data are shown in Figures S9 and S10 in the Supporting Information. Expanded photoirradiation-versus-time plots for the $x = 0.66$ and $x = 0.45$ samples are given in Figure S11 in the Supporting Information.

To make sure that the observed behavior was not due to a physical mixture of the parent compounds on a macroscopic level, a manually mixed sample of separately synthesized nickel hexacyanoferrate and cobalt hexacyanoferrate powders with $x = 0.60$ was prepared and studied (Figures S12 and S13 in the Supporting Information). For this type of synthesis, the TEM data revealed a bimodal distribution clearly associated with the two distinct sizes of the $Na_\alpha Ni[Fe(CN)_6]_\beta \cdot nH_2O$ and $Na_\alpha Co[Fe(CN)_6]_\beta \cdot nH_2O$ powders. The magnetic orderings of the two binary species were clearly visible in the $\chi(T)$ data, and the magnetization only increased with irradiation, even though the chemical composition was the same as that of the $x = 0.66$ sample that showed a photodecrease.

C. High-Temperature Magnetization. The temperature dependence of the dc magnetic susceptibility−temperature product, χT, for $T = 100-300$ K at 5 kG for various x values is shown in Figure 6a. To help ensure equilibrium during the spin crossover, a sweep rate of less than 0.5 K/min was employed. The results of the combined Bethe−Peierls−Weiss spin-crossover and Weiss mean-field magnetization calculations (described in the Supporting Information) are shown in Figure 6b. For clarity, the calculated temperature dependence of the high-spin fraction, n_{HS}, is also shown (Figure 6c).

All of the samples with $x > 0$ appear to show thermally induced CTIST, as evidenced by the abrupt reduction in the magnetic susceptibility upon cooling below ∼170 K. These CTIST events could be cycled with temperature and exhibited hysteresis that is characteristic of the cooperativity of the transition. Additionally, an evolution of the ferromagnetic slope in χT, characteristic of the $Na_\alpha Ni[Fe(CN)_6]_\beta \cdot nH_2O$ compound, as more Ni was introduced to the lattice was seen in both the numerical and experimental studies. Furthermore, the samples showed a decrease in the width of the thermal hysteresis as the amount of Co decreased as well as a drastic decrease in the amount of material undergoing CTIST as Ni was introduced into the lattice.

IV. Discussion

In the following subsections, the three main results of the experimental and numerical work performed on the ternary transition-metal Prussian blue analogue $Na_\alpha Ni_{1-x}Co_x[Fe(CN)_6]_\beta \cdot nH_2O$ are discussed. Highlighted are (1) the observation of a photoinduced decrease in magnetization, (2) the scaling of magnetic properties as a function of x, and (3) the dependence

(24) (a) Pajerowski, D. M.; Frye, F. A.; Talham, D. R.; Meisel, M. W. *New J. Phys.* **2007**, *9*, 222. (b) Frye, F. A.; Pajerowski, D. M.; Anderson, N. E.; Long, J.; Park, J.-H.; Meisel, M. W.; Talham, D. R. *Polyhedron* **2007**, *26*, 2273.

(25) We independently measured samples of $Na_jNi_k[Fe(CN)_6]_l \cdot nH_2O$ with 30 nm average edge lengths and found no significant change in the magnetization.

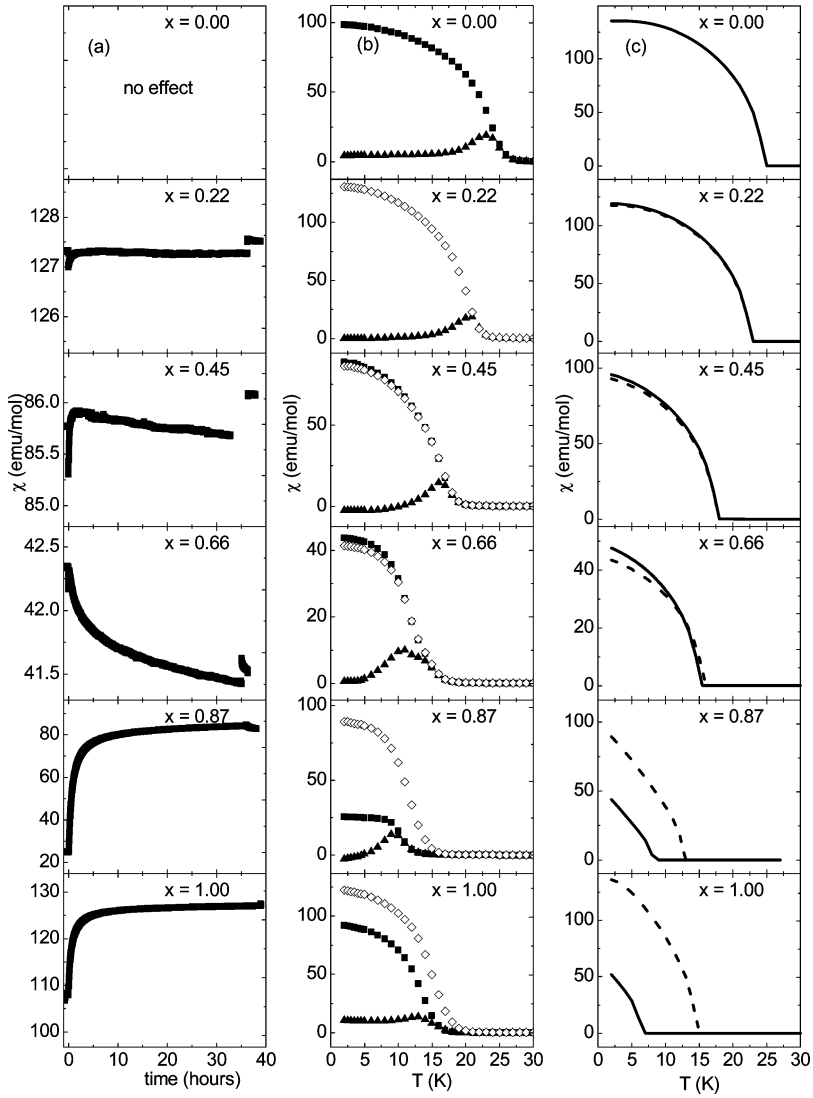

Figure 5. (a) Molar magnetic susceptibility as a function of time for samples irradiated at 5 K and 10 G, as measured in a SQUID. Discontinuities in the magnetization when the light is turned on and off are due to a subtle heating effect from the applied light. (b) Molar magnetic susceptibility as a function of temperature for both the dark FC (■) and ZFC (▲) states and the photoirradiated state (◇), as measured in a SQUID at 10 G. (c) Mean-field-calculated molar magnetic susceptibilities at 10 G as a function of temperature in the dark states (solid lines), where the high-spin fraction, n_{HS}, was determined from fitting the high-temperature susceptibility, and in the photoirradiated states (dashed lines), where $n_{HS} = 1$. The magnetic signals are expressed per mole of sample using the chemical formulas listed in Table 1.

of the observed CTIST effect upon dilution of the parent cobalt hexacyanoferrate material. Finally, aspects and potential future extensions of the mean-field calculations are examined in light of the experimental results.

A. Photoinduced Decrease in Magnetization. After the observation of a photoinduced decrease in magnetization in trilayered heterostructures of ferrimagnetic $Rb_\alpha Co[Fe(CN)_6]_\beta \cdot nH_2O$ sandwiched between two layers of ferromagnetic $Rb_\alpha Ni[Fe(CN)_6]_\beta \cdot nH_2O$,[10] calculations were developed to determine whether the photoeffects could be due to the interplay between ferromagnetic and antiferromagnetic exchange (Figure 1). Preliminary numerical results were consistent with our conjecture, but the thin-film geometry and the quaternary formula obfuscated the results. This early work sparked the numerical studies of the nickel−cobalt−iron compound presented in this report, which also predict a photoinduced decrease in magnetism.

The mean-field calculations predict a decrease in magnetization within the ordered state with increasing high-spin fraction for $Na_\alpha Ni_{1-x}Co_x[Fe(CN)_6]_\beta \cdot nH_2O$ powders with enough ferromagnetic Ni^{II} constituent ions. These predictions are compared to low-temperature magnetic susceptibility experiments as a function of x. All of the samples show an increase in magnetization at high field (Figure S9 in the Supporting Information), even those showing the photodecrease at low field (Figure 5). This increase in magnetization at high field regardless of x proves that additional spins are being generated rather than destroyed during photoirradiation. These results also indicate that the mechanism of the photoinduced magnetization, which is present in all of the samples having $x > 0$, is the same CTIST leading to persistent long-lived metastable states as seen in the pure $Rb_\alpha Co[Fe(CN)_6]_\beta \cdot nH_2O$ material. The photoeffect can be reproduced and reversed with thermal cycling above ~150 K. The ability of the mean-field calculations to predict whether a material will have a photoincrease or photodecrease based upon its composition (Figure 5) substantiates our claim that the observed photoinduced decreases in magnetization can be

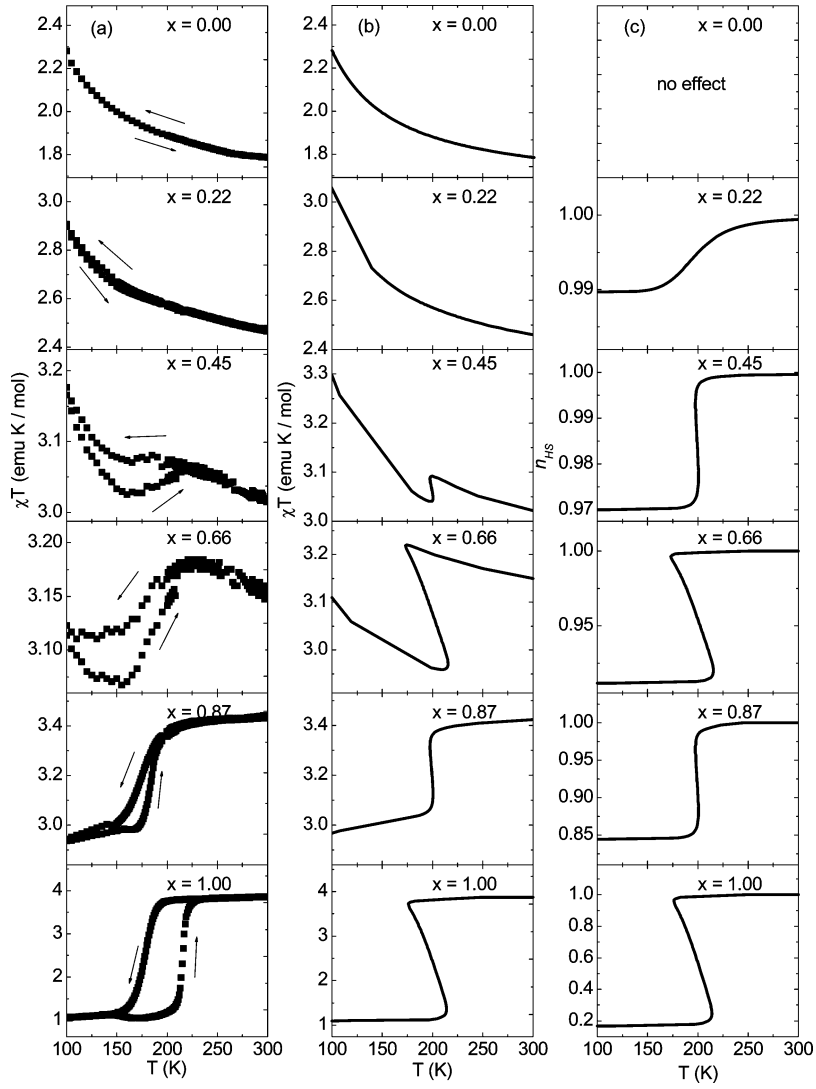

Figure 6. (a) χT vs T as measured in a SQUID magnetometer with a 5 kG applied field. The results of mean-field calculations for (b) χT vs T and (c) the high-spin fraction, n_{HS}, vs T are also shown. The magnetic signals are expressed per mole of sample using the chemical formulas listed in Table 1.

understood as an interplay between ferromagnetic and antiferromagnetic superexchange interactions, as was hypothesized in Figure 1.

These points can be further elucidated by focusing on the $x = 0.66$ sample. This sample has enough ferromagnetically interacting nearest neighbors to begin driving the Fe sublattice parallel to the applied field, while it simultaneously possesses enough Co−NC−Fe switchable pairs to still show an appreciable CTIST effect. In the low-field limit, newly photoexcited Co−NC−Fe pairs align antiparallel to the applied field as a result of the antiferromagnetic superexchange between Co and Fe ions. Since the Fe ions are already parallel to the field because of the presence of Ni, a net photodecrease in magnetization is observed (Figure 7). When a sufficiently high external magnetic field is applied, the energy reduction gained by aligning Co−NC−Fe pairs with the applied field is larger than the superexchange, so a net photoincrease in magnetization is measured (Figure 7). The temperature dependence of both the experimental and numerical magnetizations in the low-field limit shows a decrease in the measured susceptibility below ~12 K, above which an increase is observed because the thermal energy is now able to populate the excited states having Co spins parallel to the applied field.

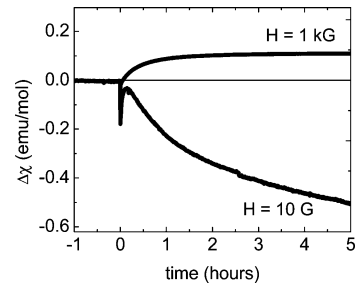

Figure 7. Photoinduced change in susceptibility for the $x = 0.66$ sample at $T = 5$ K measured at low field ($H = 10$ G) and high field ($H = 1$ kG). Photoirradiation was continuous for $t > 0$.

We should also note that the photoinduced magnetic effect shows a time dependence on the scale of weeks. For example, when the samples were measured again after 1 month in a freezer at T ≈ 248 K, the photodecrease was found to be slightly stronger by a few percent. This evolution of the magnetic properties may be due to an increase of atomic mixing of the samples arising from solid-state diffusion or to stabilization of the positions of interstitial counterions to regions more prone to induce bistabilities in the spin states.

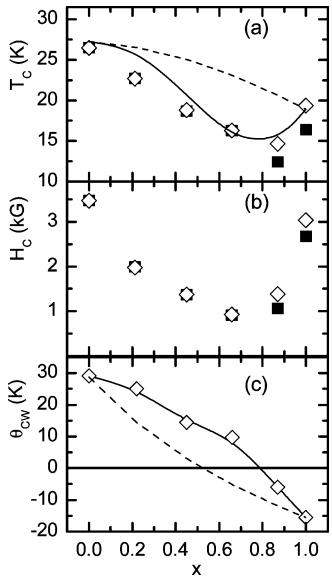

Figure 8. (a) Magnetic critical temperature T_C, (b) coercive field H_C, and (c) Curie−Weiss temperature θ_{CW} for the "low-spin" (■) and "high-spin" (◇) states as functions of x. Dashed lines are mean-field interpolations between the two pure materials. Solid lines are from mean-field fits of θ_{CW} that allow for a modification of exchange constants as the M−NC−M′ distance changes as a function of x; superexchange constants were empirically scaled to 80% of their fit values for comparison to the low-temperature T_C values. Coercive fields were obtained at $T = 2$ K after sweeping the field to 70 kG. Curie−Weiss temperatures were obtained by fitting from 250 to 300 K, where n_{HS} and μ_{eff} are essentially constant.

As a final point, the expectation of a photoeffect having the sign opposite that of the pure PBA material because of a mixing of ferromagnetic and antiferromagnetic superexchange interactions is similar to the photoinduced magnetic-pole inversion reported for the PBA $(Fe_{1-x}Mn_x)_{1.5}[Cr(CN)_6]\cdot nH_2O$.[11b] A fundamental difference, however, is that in the $(Fe_{1-x}Mn_x)_{1.5}[Cr(CN)_6]\cdot nH_2O$ system, the applied light destroys exchange pathways, whereas additional moments are generated in the $Na_\alpha Ni_{1-x}Co_x[Fe(CN)_6]_\beta\cdot nH_2O$ system reported here.

B. Scaling of Magnetic Properties. All of the $Na_\alpha Ni_{1-x}Co_x[Fe(CN)_6]_\beta\cdot nH_2O$ samples studied showed spin-glass-like long-range magnetic order, as evidenced by the bifurcation of the FC and ZFC curves (Figure 5b). The peak in the ZFC susceptibility is a fingerprint of the spin-glass-like nature of the order in both parent compounds,[26,27] the presence of which hints at the complicated nature of the magnetism in the samples investigated. It is noteworthy that local minima are present near $x \approx 0.8$ in the scaling of the magnetic ordering temperature, the coercive field, and the absolute value of the Curie−Weiss temperature as a function of x (Figure 8).

Our observed scaling of magnetic properties in $Na_\alpha Ni_{1-x}Co_x[Fe(CN)_6]_\beta\cdot nH_2O$ can be compared with previous work on ternary transition-metal PBAs.[13,28] In ternary materials of $Cu[Co_xFe_{1-x}(CN)_6]$, $Ni[Co_xFe_{1-x}(CN)_6]$, and $Fe[Co_xFe_{1-x}(CN)_6]$, a clear monotonic scaling of the transition temperature with x was observed, and these results are dominated by the changing number of magnetic nearest neighbors, since Co^{III} on the M site is LS and therefore diamagnetic.[28a] Similar monotonic scaling was observed in $Ni[Cr_xFe_{1-x}(CN)_6]$ and $Fe[Cr_xFe_{1-x}(CN)_6]$,[28b] where the substitution of Cr^{III} ($S = {}^3/_2$) for Fe^{III} ($S = {}^1/_2$) provides a 3-fold increase in the number of superexchange pathways, since the number of unpaired t_{2g} electrons on the M site changes from one to three $[(t_{2g})^5 \rightarrow (t_{2g})^3]$. Finally, the most cogent example is $(Ni_xMn_{1-x})_{1.5}[Cr(CN)_6]\cdot nH_2O$, which displays a clear dip in the ordering temperature and a peak in the coercive field on the background of a linear dependence from interpolation between the values of the parent compounds as x changes.[13] A few similarities are obvious when comparing $Na_\alpha Ni_{1-x}Co_x[Fe(CN)_6]_\beta\cdot nH_2O$ and $(Ni_xMn_{1-x})_{1.5}[Cr(CN)_6]\cdot nH_2O$, particularly in the context of simple empirical rules for superexchange.[29a] First, both contain a Ni^{II} ion that has a ferromagnetic superexchange pathway (e_g to t_{2g}). Second, the interaction between Mn^{II} and Cr^{III} is analogous to the Co^{II} interaction with Fe^{III} in $Na_\alpha Ni_{1-x}Co_x[Fe(CN)_6]_\beta\cdot nH_2O$, as there is a competition between ferromagnetic and antiferromagnetic interactions (Figure 9a). It is plausible that when two superexchange energies of opposite sign compete, the net magnetic interaction is particularly susceptible to perturbation when the interion distance is changed. The nonmonotonicities observed in the ordering temperatures as a function of metal substitution may therefore be due to a net superexchange that depends strongly on the small distance changes that are introduced with the substitution. In order to reproduce our experimental data, it was necessary to introduce a distance dependence into the Co^{II}(HS)−NC−Fe^{III}(LS) superexchange interaction (Figure 9b).

The need to introduce distance dependence to the superexchange interaction in order to reproduce the data may seem drastic, but other methods of reproducing the scaling of the magnetic properties were unsuccessful. Two remarkable features are present in the data: the dip in the ordering temperature near $x = 0.8$ and the unexpectedly large ferromagnetic character of the mixed samples. This increase in ferromagnetic character manifests itself in the lack of a compensation point for our mixed ferro−ferrimagnetic system and in the high-temperature slope of χT for the mixed samples. Specifically, from 250 to 300 K, χT for the $x = 0.66$ sample *increased* as temperature decreased, whereas a model using the binary magnetic interactions predicts a clear *decrease* with decreasing temperature. For powder samples containing ions in similar environments to ours, the introduction of single-ion anisotropy and spin−orbit coupling terms can give rise only to a decrease in χT as temperature decreases.[29] Finally, there are precedents in the literature for such a modification of the superexchange energy. In $Cs_\alpha Co[Cr(CN)_6]_\beta\cdot nH_2O$ ferromagnetic compounds having competing ferromagnetic and antiferromagnetic pathways, a dependence of the superexchange energy on the lattice constant was found.[30] Additionally, an $A_\alpha Co[Fe(CN)_6]_\beta\cdot nH_2O$ material was reported in which ferromagnetic coupling, as opposed to the usual

(26) (a) Pejaković, D. A.; Manson, J. L.; Miller, J. S.; Epstein, A. J. *Phys. Rev. Lett.* **2000**, *85*, 1994. (b) Pejaković, D. A.; Manson, J. L.; Miller, J. S.; Epstein, A. J. *J. Appl. Phys.* **2000**, *87*, 6028. (c) Pejaković, D. A.; Manson, J. L.; Miller, J. S.; Epstein, A. J. *Synth. Met.* **2001**, *122*, 529. (d) Pejaković, D. A.; Manson, J. L.; Kitamura, C.; Miller, J. S.; Epstein, A. J. *Polyhedron* **2001**, *20*, 1435. (e) Pejaković, D. A.; Kitamura, C.; Miller, J. S.; Epstein, A. J. *Mol. Cryst. Liq. Cryst.* **2002**, *374*, 289.

(27) Phu, P. K.; Giang, T. N.; Minh, N. V. *Commun. Phys.* **2008**, *18*, 43.

(28) (a) Widmann, A.; Kahlert, H.; Petrovic-Prelevic, I.; Wulff, H.; Yakhmi, J. V.; Bagkar, N.; Scholz, F. *Inorg. Chem.* **2002**, *41*, 5706. (b) Bagkar, N.; Widmann, A.; Kahlert, H.; Ravikumar, G.; Yusuf, S. M.; Scholz, F.; Yakhmi, J. V. *Philos. Mag.* **2005**, *85*, 3659. (c) Widmann, A.; Kahlert, H.; Wulff, H.; Scholz, F. *J. Solid State Electrochem.* **2005**, *9*, 380. (d) Schwudke, D.; Stösser, R.; Scholz, F. *Electrochem. Commun.* **2000**, *2*, 301.

(29) (a) Kahn, O. *Molecular Magnetism*; Wiley-VCH: New York, 1993. (b) Lloret, F.; Julve, M.; Cano, J.; Ruiz-Garcia, R.; Pardo, E. *Inorg. Chim. Acta* **2008**, *361*, 3432. (c) Baker, J.; Figgis, B. N. *Aust. J. Chem.* **1982**, *35*, 265.

(30) Ohkoshi, S.-i.; Hashimoto, K. *Chem. Phys. Lett.* **1999**, *314*, 210.

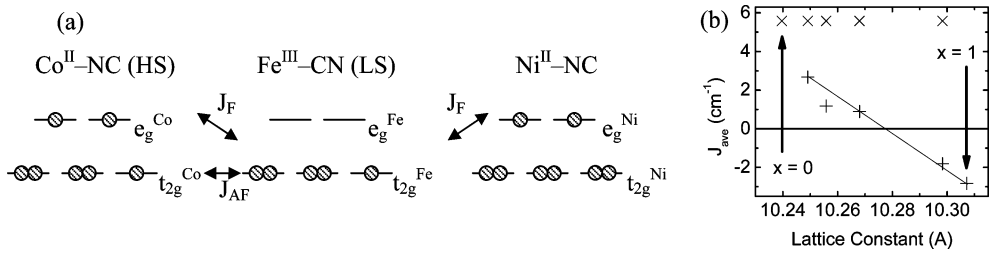

Figure 9. (a) Energy levels and diagram for the superexchange interactions considered in the material. The Co^{II}(HS) ion notably has both ferromagnetic ($J_F > 0$) and antiferromagnetic ($J_{AF} > 0$) superexchange interactions with Fe^{III}(LS), in contrast with Ni^{II}. (b) Average values of the exchange constants, J_{ave}, for the Ni^{II}−NC−Fe^{III} (×) and Co^{II}−NC−Fe^{III} (+) exchange bonds used in order to reproduce the scaling in Figure 8. The line is merely a guide for the eyes.

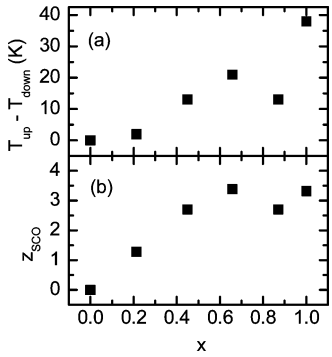

Figure 10. (a) Width of the thermal hysteresis, $T_{up} - T_{down}$ and (b) number of spin-crossover-active nearest neighbors, z_{SCO}, as a function of x. Here, $T_{up} - T_{down}$ is defined as the difference in the temperature at which half of the spin-crossover-active material is high-spin when sweeping up in temperature and that at which half of the spin-crossover-active material is high-spin when sweeping down in temperature.

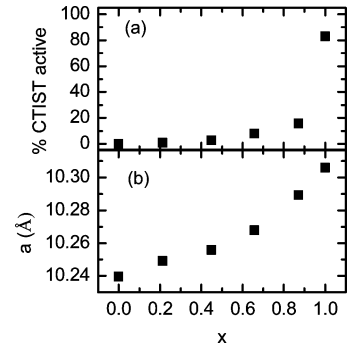

Figure 11. (a) Percentage of CTIST-active material and (b) unit-cell lattice constant a as functions of x.

*anti*ferromagnetic coupling leading to a ferrimagnet, was inferred on the basis of the high-temperature inverse susceptibility.[14]

C. Spin-Crossover Dilution. The width of the thermal hysteresis, as represented by $T_{up} - T_{down}$, decreases when the cobalt hexacyanoferrate material is diluted, and this trend is correlated with the number of active CTIST nearest neighbors, z_{SCO} (Figure 10). As described in the Supporting Information, z_{SCO} can be calculated from the chemical formula, and the observed narrowing of the hysteresis is an expected result when z_{SCO} decreases. It is worth noting that while the changing number of nearest neighbors is a dominant effect, additional perturbations due to the changing of the local environments of the active species are also present. Experimentally, the dilution of spin-crossover species has been intensively investigated since its first realization in $[Fe_xZn_{1-x}(2\text{-pic})_3]Cl_2 \cdot EtOH$,[31] where a gradual reduction in the width of the hysteresis loop was attributed to the many-body elastic interactions innate to these transitions. With respect to CTIST in PBAs, the field is not as mature, and studies are still ongoing. Recently, a CTIST diluted $Rb_{0.70}Cu_{0.22}Mn_{0.78}[Fe(CN)_6]_{0.86} \cdot 2.05H_2O$ sample was compared to its undiluted parent compound $Rb_{0.81}Mn[Fe(CN)_6]_{0.95} \cdot 1.24H_2O$, and no appreciable change in the width of the hysteresis loop was observed.[32]

Furthermore, there is a striking reduction in the amount of CTIST-active material once nickel is introduced into the lattice (Figure 11a). More specifically, the $x = 1.00$ material transitions 83% of the amount expected from the chemical formula when T is swept from 300 to 100 K, whereas the $x = 0.87$ material transitions 16% of the expected amount and the samples with smaller x values transition less than 10%. The percent of CTIST-active material can be established by considering the chemical formula, the room-temperature FT-IR spectrum, and the change in χT as the samples are cooled. Although a detailed investigation of the microscopic origins of the observed reduction in spin-crossover-active material is warranted, we conjecture that this reduction is related to a Ni-induced stabilization of Co−NC−Fe HS pairs arising from subtle variations of the unit cell parameters (Figure 11b). The lattice constants are observed to scale with x in a monotonic fashion that is consistent with changes seen in other ternary metal PBAs.[13,28] However, the nonlinear nature of the scaling implies an actual change in the bond energies of the system as the different systems are mixed. The FT-IR data also provide evidence supporting the stabilization of the coordination bond upon incorporation of Ni^{II}. For the cyanide stretch associated with the divalent metal to iron bond, plots of the stretching frequency and an effective spring constant as functions of x can be made (Figure 12), and these imply a stabilization of the bond and an increased rigidity of the lattice upon introduction of nickel ions. Therefore, it may no longer be energetically favorable for Co−NC−Fe pairs in $Na_\alpha Ni_{1-x}Co_x[Fe(CN)_6]_\beta \cdot nH_2O$ to undergo CTIST because of the added strain that would result for the Ni−NC−Fe bonds in the system. More specifically, the LS phase of $Na_\alpha Co[Fe(CN)_6]_\beta \cdot nH_2O$ has a lattice constant of 9.9721 Å, whereas the HS phase has a lattice constant of 10.3033 Å,[5g] which is comparable to the lattice constant of 10.30(7) Å in the $x = 1.00$ sample. In contrast, the $x = 0.00$ nickel hexacyanoferrate species has a lattice constant of 10.23(9) Å, which is comparable to the previously reported value of 10.229 Å for $Ni_3[Fe(CN)_6]_2$.[14]

(31) (a) Sorai, M.; Ensling, J.; Gütlich, P. *Chem. Phys.* **1976**, *18*, 199. (b) Spiering, H.; Meissner, E.; Köppen, H.; Müller, E. W.; Gütlich, P. *Chem. Phys.* **1982**, *68*, 65.

(32) (a) Lummen, T. T. A.; Gengler, R. Y. N.; Rudolf, P.; Lusitani, F.; Vertelman, E. J. M.; van Koningsbruggen, P. J.; Knupfer, M.; Molodtsova, O.; Pireaux, J.-J.; van Loosdrecht, P. H. M. *J. Phys. Chem. C* **2008**, *112*, 14158.

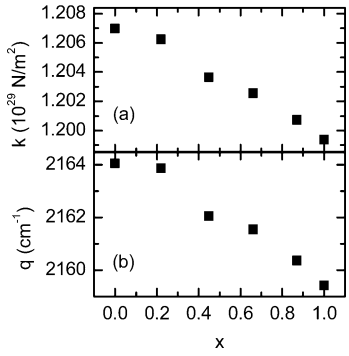

Figure 12. (a) Effective spring constant and (b) FT-IR frequency for the CN stretch in $M^{II}-CN-Fe^{III}$ as functions of x.

Comparisons of our observation of the reduction in the amount of CTIST-active material to the results of a recent work studying the dilution of cobalt hexacyanoferrate by diamagnetic Zn^{II} at the divalent metal site or by diamagnetic Co^{III} at the cyanometallate site[12] are useful. In particular, a similar sensitivity of the CTIST effect to metal substitution was seen by Cafun et al.,[12] and the reduction in the magnitude of the effect in their samples is also larger than expected for a simple reduction in the spin-crossover-active species on a molecule-by-molecule level. It was previously shown by Ksenofontov et al.[33] that application of hydrostatic pressure to $A_\alpha Co[Fe(CN)_6]_\beta \cdot nH_2O$ powders induced a stabilization of the LS phase in the samples. This leads to the obvious contention that the stabilization of the high-spin phase for $Na_\alpha Ni_{1-x}Co_x[Fe(CN)_6]_\beta \cdot nH_2O$ may simply be due to an effective "negative pressure." It was suggested[12] that the observed stabilization with metal substitution could not be due to such an effect because their starting material had a cell size of ~10.32 Å; thus, while the 100% Zn^{II}-doped material should have a negative pressure because of its cell size of ~10.40 Å, the 100% $Co^{III}(CN)_6$-doped material should have a positive pressure because of its lattice constant of ~10.23 Å. However, these room-temperature values all deal with the high-spin lattice constants, but with respect to the low-spin lattice constants, the alien species are still larger than the LS Co−NC−Fe state and in fact closer in size to the HS Co−NC−Fe state than the LS Co−NC−Fe state, suggesting that chemical pressure may still be a valid argument for the effect. Finally, more subtle effects on the energy of the cobalt−iron charge transfer arising from the presence of neighboring nickel ions may also be present.

D. Mean-Field Predictions versus Observations. The mean-field calculations were able to predict whether the magnetization of the chosen samples would increase or decrease with photoirradiation. Upon completion of the experiments, the lack of a compensation point and subsequent negative magnetization, as well as the general scaling of magnetic properties, was surprising. However, a better agreement between calculations and experiment was found when a distance dependence was introduced into the superexchange constant. In addition, discrepancies between predictions and experiment may have stemmed from the need to choose the simplest Hamiltonian that could capture the spirit of the problem, which had only Zeeman and superexchange terms, in order to make the number of free parameters tractable. Nevertheless, it is worth stating clearly that the two main results, a photoinduced decrease in magnetization for certain values of x and a reduction in the amount of the CTIST-active material with metal substitution, are qualitatively robust with respect to perturbations of the model. A future study might consider single-ion anisotropies on the Co and Ni sites, as in recent reports in which more complicated Hamiltonians for ternary PBAs have been solved by mean-field[34a] and Monte Carlo methods.[34b]

V. Conclusions

We have demonstrated that the ternary transition-metal Prussian blue analogue $Na_\alpha Ni_{1-x}Co_x[Fe(CN)_6]_\beta \cdot nH_2O$ shows a photoinduced decrease in magnetization for certain values of x, temperature, and applied magnetic field. Furthermore, the $Na_\alpha Ni_{1-x}Co_x[Fe(CN)_6]_\beta \cdot nH_2O$ system is the first example of a compound in which superexchange energies control whether incident light increases or decreases CTIST magnetization. As a result, the sign of the photoeffect can be changed by stoichiometry. Although a photoinduced decrease in magnetization with an increase in the number of spins has also been seen in $A_\alpha Co[Fe(CN)_6]_\beta \cdot nH_2O$ thin films,[8a] the microscopic origins are different. In addition, the width of the thermal hysteresis of the CTIST is reduced upon dilution of the spin-crossover-active species in the ternary mixture. The origins of the experimental observations are nicely explained using mean-field calculations.

Acknowledgment. This work was supported in part by NSF DMR-0701400 (M.W.M.) and NSF DMR-0453362 (D.R.T.). We sincerely thank Ben Pletcher and the Major Analytical Instrumentation Center (MAIC), Department of Materials Science and Engineering, University of Florida, for the TEM images and the EDS data.

Supporting Information Available: Powder XRD patterns with fits and fitting parameters, further description of the mean-field calculations, color dependence, details of FT-IR extinction coefficient calibration, FT-IR spectra with fits and fitting parameters, full-field sweeps used to determine the magnetization at 70 kG and the coercive fields, a check for symmetry of the hysteresis loop, expanded χ-versus-time plots for $x = 0.45$ and $x = 0.66$ samples, TEM micrographs from the control study done on separately synthesized and subsequently mixed compounds, and the dark and photoirradiated magnetic susceptibilities of a manually mixed powder. This material is available free of charge via the Internet at http://pubs.acs.org.

JA9012672

(33) Ksenofontov, V.; Levchenko, G.; Reiman, S.; Gütlich, P.; Bleuzen, A.; Escax, V.; Verdaguer, M. *Phys. Rev. B* **2003**, *68*, 024415.
(34) (a) Bobák, A.; Abubrig, F. O.; Balcerzak, T. *Phys. Rev. B* **2003**, *68*, 224405. (b) Dely, J.; Bobák, A.; Horváth, D. *Acta Phys. Pol., A* **2008**, *113*, 461.